AGU PUBLICATIONS

JGR

Journal of Geophysical Research: Oceans

RESEARCH ARTICLE

10.1002/2015JC011386

Key Points:
- The optimal precursory disturbances for El Niño and La Niña events are identified
- The optimal precursory disturbances and optimally growing initial errors exhibit similarities
- The implications of these similarities to target observations are discussed

Correspondence to:
W. Duan,
duanws@lasg.iap.ac.cn

Citation:
Hu, J., and W. Duan (2016), Relationship between optimal precursory disturbances and optimally growing initial errors associated with ENSO events: Implications to target observations for ENSO prediction, *J. Geophys. Res. Oceans*, *121*, doi:10.1002/2015JC011386.

Received 9 OCT 2015
Accepted 27 MAR 2016
Accepted article online 31 MAR 2016

Relationship between optimal precursory disturbances and optimally growing initial errors associated with ENSO events: Implications to target observations for ENSO prediction

Junya Hu[1,2] and Wansuo Duan[1,3]

[1]State Key Laboratory of Numerical Modeling for Atmospheric Sciences and Geophysical Fluid Dynamics (LASG), Institute of Atmospheric Physics, Chinese Academy of Sciences, Beijing, China, [2]University of Chinese Academy of Sciences, Beijing, China, [3]Ningbo Collaborative Innovation Center of Nonlinear Hazard System of Ocean and Atmosphere, Ningbo University, Ningbo, China

Abstract By superimposing initial sea temperature disturbances in neutral years, we determine the precursory disturbances that are most likely to evolve into El Niño and La Niña events using an Earth System Model. These precursory disturbances for El Niño and La Niña events are deemed optimal precursory disturbances because they are more likely to trigger strong ENSO events. Specifically, the optimal precursory disturbance for El Niño exhibits negative sea surface temperature anomalies (SSTAs) in the central-eastern equatorial Pacific. Additionally, the subsurface temperature component exhibits negative anomalies in the upper layers of the eastern equatorial Pacific and positive anomalies in the lower layers of the western equatorial Pacific. The optimal precursory disturbance for La Niña is almost opposite to that of El Niño. The optimal precursory disturbances show that both El Niño and La Niña originate from precursory signals in the subsurface layers of the western equatorial Pacific and in the surface layers of the eastern equatorial Pacific. We find that the optimal precursory disturbances for El Niño and La Niña are particularly similar to the optimally growing initial errors associated with El Niño prediction that have been presented in previous studies. The optimally growing initial errors show that the optimal precursor source areas represent the sensitive areas for target observations associated with ENSO prediction. Combining the optimal precursory disturbances and the optimally growing initial errors for ENSO, we infer that additional observations in these sensitive areas can reduce initial errors and be used to detect precursory signals, thereby improving ENSO predictions.

1. Introduction

ENSO is an irregular interannual oscillation that alternates between the warm (El Niño) and cold (La Niña) phase as a result of coupled ocean-atmosphere interactions in the tropical Pacific [*Rasmusson and Carpenter*, 1982; *Philander*, 1983, 1990]. ENSO has a far-reaching impact on climate through teleconnections; hence, accurate ENSO predictions are essential for producing meaningful seasonal climate predictions globally [*Ropelewski and Halpert*, 1987; *Trenberth et al*., 1998]. In recent decades, ENSO predictions have made significant progress. Skillful predictions can be made 1 year in advance in hindcast experiments [*Chen and Cane*, 2008; *Jin et al*., 2008]. However, considerable uncertainties still exist in real-time ENSO forecasting [*Kirtman et al*., 2002; *Tippett et al*., 2012], especially those associated with poor predictive ability during the ENSO onset period. One approach utilizes precursory signals that precede the onset of ENSO events. These signals can be used to predict ENSO events with significant lead times [*Yu and Paek*, 2015].

Multiple studies have investigated the precursors of ENSO events using optimal perturbations. For example, *Moore and Kleeman* [1996] explored the precursors of ENSO using the linear singular vector (LSV) approach. They demonstrated that a downward-perturbed thermocline pattern in the equatorial Pacific has the potential to develop into an El Niño event [also see *Xue et al*., 1994; *Palmer et al*., 1994]. *Thompson* [1998] obtained similar results using the LSV approach. In addition, *Newman et al*. [2011] and *Vimont et al*. [2014] used linear inverse models (LIM) to determine optimal initial conditions for an El Niño event. Specifically, a positive, basin-wide thermocline anomaly centered in the central-eastern Pacific and an SSTA along the coast of Peru will likely evolve into an El Niño event. The opposite conditions provide optimal initial conditions for a

La Niña event. However, these results are based on a linear approximation of the nonlinear, tropical ocean-atmosphere system. This approximation is incapable of depicting the effects of nonlinearities associated with the relevant nonlinear physical processes. Therefore, the linear approach is limited when used to describe the precursory disturbances for ENSO events.

To overcome the limitations of linear approaches, *Mu et al*. [2003] proposed a novel approach of conditional nonlinear optimal perturbation (CNOP). This method involves nonlinearity and can be used to describe the nonlinear evolution of finite-amplitude initial perturbations. CNOP represents the optimal initial perturbation that has the largest nonlinear evolution at the end of the optimization. If CNOP is superimposed on a climatological annual cycle, it acts as an initial anomaly that is most likely to evolve into a climate event, i.e., the optimal precursory disturbance for the climate event. In terms of ENSO, CNOP can represent an optimal precursory disturbance. *Duan et al*. [2013] applied the CNOP approach to the Zebiak-Cane model of intermediate complexity [*Zebiak and Cane*, 1987] to identify the optimal precursory disturbances for El Niño events. They illustrated that the SSTA component of the optimal precursory disturbance associated with El Niño exhibits a zonal dipole pattern with positive anomalies in the eastern equatorial Pacific and negative anomalies in the central equatorial Pacific, plus a deepening thermocline depth along the equatorial Pacific. In particular, the thermocline depth fluctuation precedes the SST changes in the equatorial Pacific, which has also been observed in previous studies [*Wyrtki*, 1975, 1985; *Mu and Li*, 2000; *Duan et al*., 2004]. Nevertheless, the Zebiak–Cane model is a simple anomaly model and is unable to address some observed processes, such as wind anomalies in the western North Pacific and seasonal variations of the mean thermocline depth in the equatorial Pacific [*An and Wang*, 2001]. Consequently, the model possesses limitations associated with reproducing ENSO events, especially nonphase-locked La Niña events. Therefore, results obtained using the Zebiak–Cane model should be verified by a more complete Earth System Model. In particular, the precursory disturbances for La Niña events are expected to be accurately determined. The Community Earth System Model (CESM) of the National Center for Atmospheric Research (NCAR) is adopted in this paper to explore the precursory disturbances for El Niño and especially reveal precursors for La Niña events. These findings are then compared with those obtained using the Zebiak–Cane model.

In addition, uncertainties in ENSO predictions are caused by initial errors, forecast model flaws and stochastically driven errors [*Chen and Cane*, 2008; *Lopez and Kirtman*, 2014; *Larson and Kirtman*, 2015]. Many studies have explored the impact of initial errors on ENSO predictions [*Moore and Kleeman*, 1996; *Samelson and Tziperman*, 2001; *Chen et al*., 2004; *Mu et al*., 2007a, 2007b; *Duan et al*., 2009; *Yu et al*., 2009]. *Duan and Hu* [2015] explored the optimally growing initial errors (OGEs) that often cause a significant "spring predictability barrier" (SPB) for El Niño events and determined the sensitive areas for ENSO prediction using the CESM model. They demonstrated that there are two types of OGEs. One type exhibits negative SST anomalies in the central-eastern equatorial Pacific and a basin-wide dipolar pattern of the subsurface temperature anomaly, with negative anomalies in the upper layers of the eastern equatorial Pacific and positive anomalies in the lower layers of the western equatorial Pacific. The other type consists of an SSTA component with positive anomalies in the southeastern equatorial Pacific and a large-scale zonal dipole pattern of the subsurface temperature anomaly, with positive anomalies in the upper layers of the eastern equatorial Pacific and negative anomalies in the lower layers of the central-western equatorial Pacific [see *Duan and Hu*, 2015, Figure 6]. To facilitate the following discussion, we refer to the former error pattern as a type-1 OGEs and the latter as a type-2 OGEs. On the basis of OGEs, *Duan and Hu* [2015] identified the sensitive areas for target observations associated with El Niño prediction as the lower layers of the western equatorial Pacific and the upper layers of the eastern equatorial Pacific. Numerical experiments have confirmed that El Niño forecasting can be greatly improved when the initial errors in these sensitive areas (as compared with other regions) are eliminated. Are precursory disturbances for ENSO events related to these OGEs? If so, what useful information can their relationships provide for improving ENSO forecasting? To address these questions, we first characterize the precursory disturbances for ENSO events. We then explore their relationships with the OGEs of ENSO prediction and present the associated implications.

The remainder of the paper is organized as follows. Section 2 includes a brief description of the CESM model and a validation for the tropical Pacific. Section 3 reviews the CNOP approach and introduces the specific experimental strategy implemented using the CESM model. Section 4 presents the precursory disturbances for El Niño and La Niña events. Section 5 investigates the relationship between the precursory disturbances and OGEs as well as the associated implications. Finally, a conclusion and a discussion are presented in Section 6.

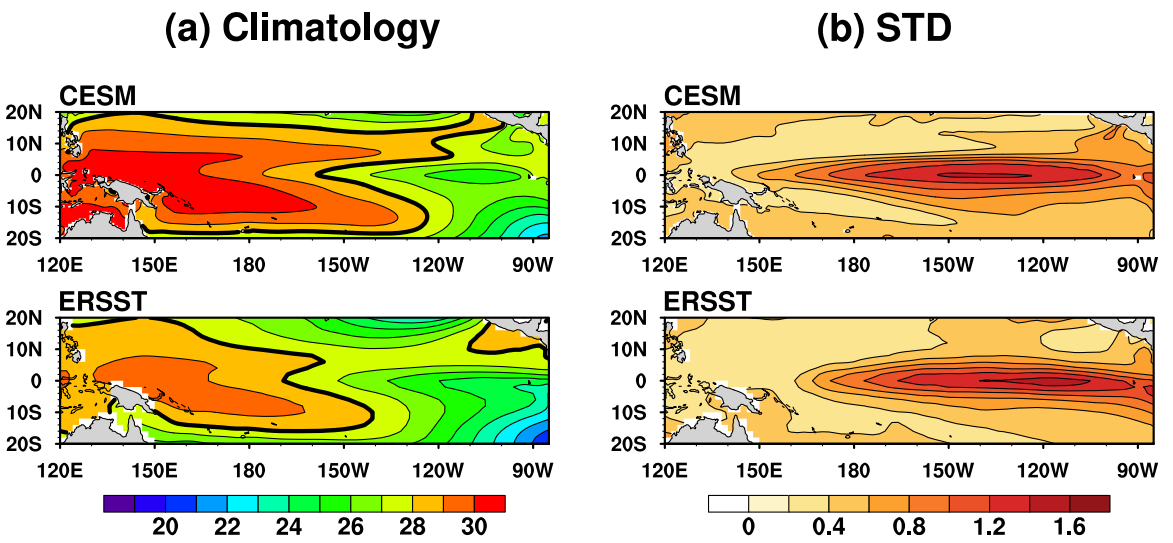

Figure 1. (a) Climatology of SSTs (°C) over the tropical Pacific during ND(0)J(1) based on the CESM 100 year simulations and 1952–2011 observations from the Extended Reconstructed Sea Surface Temperature version 3 (ERSST V3) data set [*Smith et al*., 2008]. The thick black lines indicate the 28°C isotherm. (b) Standard deviation of SST anomalies (°C) from the CESM 100 year simulations and 1952–2011 ERSST V3 observations.

2. Model Description and Validation

The Earth System Model adopted in this study is the Community Earth System Model (CESM), which combines the Parallel Ocean Program version 2 (POP2) ocean model of Los Alamos National Laboratory and the Community Atmosphere Model version 4 (CAM4) atmospheric model. CAM4 and POP2 are further combined with the Community Land Model version 4.0 (CLM4) [*Oleson et al*., 2010], the Los Alamos sea ice model, referred to as the Community Ice CodE version 4.0 (CICE4) [*Hunke and Lipscomb*, 2008], and a dynamic ice sheet model known as Glimmer-CISM [*Rutt et al*., 2009; *Lipscomb et al*., 2013] through the version 7 coupler (CPL7) [*Craig et al*., 2012]. The standard horizontal resolution of POP2 is approximately 1° (longitude) × 1° (latitude) with a displaced pole grid. However, a local transformation is applied to the grid in the tropics to refine the meridional resolution to approximately 0.27° at the equator. The model has 60 vertical levels. The layer spacing is 10 m in the upper 160 m and increases to 250 m by a depth of approximately 3500 m. The spacing remains constant below this depth. CAM4 has a finite-volume (FV) dynamical core with 26 vertical layers. The horizontal resolution of the regular longitude–latitude grid is 0.9° (longitude) × 1.25° (latitude) [*Neale et al*., 2013]. The CESM consists of component models that can be combined in different configurations, creating a wide variety of options for different model configurations and resolutions [*Hurrell et al*., 2013]. More details of the CESM coupling infrastructure are given in *Craig et al*. [2012].

In this study, a 150 year control integration was performed using CESM. Tracer gases, insolation, aerosols and land cover during the year 2000 were used as forcing parameters. The last 100 years of integrations are used in this study, allowing for an initial adjustment during the model simulation. Figure 1 shows the winter mean SST and standard deviation of interannual SST anomalies in November-January, which encompasses the peak phase of ENSO events. The simulated SST and interannual variability are comparable to observations; however, the typical systematic bias associated with the warm pool extends too far east of the dateline. Additionally, the area of strong CESM variability shifts slightly westward. These issues are common in coupled global climate models [*AchutaRao and Sperber*, 2002]. In addition, Figure 2 illustrates the Niño3 (150°W–90°W; 5°N–5°S) SST anomalies as well as the warm water volume (WWV) anomalies based on the CESM simulations. The depth of the 20°C isotherm, denoted by Z20, is used to estimate the thermocline depth. The WWV is determined by spatially integrating Z20 over the region of 5°N–5°S and 130°E–85°W. The warm and cold phases of ENSO occurred irregularly, with a dominant period of 3 years based on the wavelet analysis (not shown). As in the observations [*Meinen and McPhaden*, 2000; *McPhaden*, 2003], the WWV anomalies generally precede Niño3 SST variations (Figure 2a). The peak correlation occurs with WWV leading Niño3 by 8–9 months, as observed in the cross correlation between the two time series (Figure 2b). The lead-lag correlations between the equatorial Z20 and SST anomalies averaged at 5°S and 5°N are also

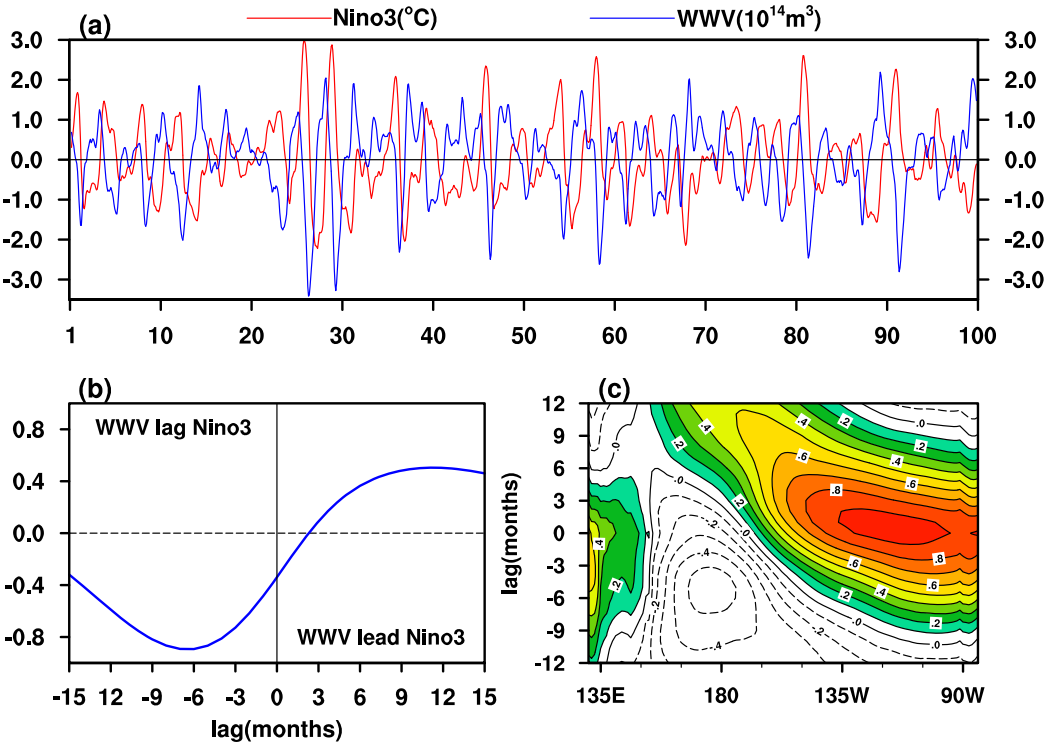

Figure 2. (a) Monthly Niño3 SST (red) and WWV (blue) anomaly time series from the 100 year model simulation. Time series have been smoothed using a 5 month running mean filter. (b) Cross correlation of monthly WWV and Niño3 SST anomalies. Positive lag suggests that WWV leads SST. (c) Lead-lag correlation coefficient between Z20 and SST anomalies averaged between 5°S and 5°N. Positive lag suggests that Z20 leads SST.

presented in Figure 2. Consistent with observations, the Z20 anomalies lead SST variations in time, with the time lag of the maximum positive correlations increasing westward (Figure 2c) [e.g., *Zelle et al*., 2004; *Wen et al*., 2014; *Zhu et al*., 2015]. In the eastern Pacific, the Z20 and SST anomalies vary almost simultaneously, while a time lag of approximately 1 year exists between the Z20 and SST anomalies in the central Pacific.

3. Approach and Experimental Strategy

To explore the precursory disturbances for ENSO events, we use the CNOP approach [*Mu et al*., 2003; *Duan and Mu*, 2009]. CNOP can be used to determine the initial anomalies that are most likely to evolve into ENSO events [*Duan and Mu*, 2009; *Duan et al*., 2013]. CNOP is an extension of LSV in a nonlinear regime. LSV cannot distinguish the effects of nonlinear physical processes. In addition, the method can only describe sufficiently small initial perturbations. CNOP is derived directly from the nonlinear model without approximations; thus, it can effectively describe the nonlinear evolution of finite-amplitude initial perturbations. CNOP exhibits significantly larger growth than LSV. In addition, the spatial patterns of CNOPs and those of LSVs are different due to the effects of nonlinearities. In terms of ENSO, *Duan et al*. [2004, 2013] demonstrated that because LSV does not recognize the fastest growing initial perturbation of the nonlinear ENSO system, the precursory disturbance obtained by LSV evolves into a much weaker ENSO event compared to the disturbance obtained by CNOP. In addition, compared to the large-scale spatial patterns of CNOP, LSV generally covers a narrower SSTA region and possesses a relatively smaller thermocline depth anomaly in the Zebiak–Cane model [*Duan et al*., 2013]. Therefore, LSV is not the most sensitive initial perturbation, limiting the identification of the optimal precursory disturbance for ENSO. CNOP is generally more capable of determining the nonlinearities associated with ENSO and optimal ENSO precursors. In the following paragraphs, we will briefly review the CNOP methodology.

Let M_t be a propagator (i.e., numerical model) of a nonlinear model that propagates an initial value to future time t. A basic state $U(t)$ that is a numerical solution to the nonlinear model must satisfy $U(t)=M_t(U_0)$ at

time t, with U_0 being the initial value of $U(t)$. If an initial perturbation u_0 is superimposed on the basic state, then the following relationship is produced:

$$U(t)+u(t)=M_t(U_0+u_0), \tag{1}$$

where $u(t)$ describes the evolution of the initial perturbation u_0.

CNOP, denoted by $u_{0\delta}$, can be obtained by solving the following nonlinear optimization problem:

$$J(u_{0\delta}) = \max_{\|u_0\|\le\delta} J(u_0) = \max_{\|u_0\|\le\delta} \|M_t(U_0+u_0)-M_t(U_0)\|, \tag{2}$$

where $\|u_0\| \le \delta$ is the constraint condition defined by the chosen norm $\|\cdot\|$, which constrains the amplitude of initial perturbations. We use the norm and the related inequality to define the constraint condition. The constraint condition could also be established based on the physical laws of a functional set that the initial perturbation satisfies.

Generally, by considering the negative cost function $J(u_0)$ to transform equation (2) into a minimization problem, the CNOP can be computed using some ready solvers, such as the Sequential Quadratic Programming (SQP) [*Powell*, 1982] and Spectral Projected Gradient 2 (SPG2) solvers [*Birgin et al.*, 2000], which are used to solve nonlinear minimization problems. These solvers require the gradient of the modified cost function. The adjoint of the corresponding model is typically used to obtain the gradient. However, most complex coupled global climate models, including CESM, do not have adjoints. As a result, it is difficult for the complex models to directly calculate CNOP using the adjoint model. *Duan et al.* [2009] proposed an ensemble-based algorithm to approximate CNOP without using adjoint models. The Zebiak–Cane model results are physically reasonable and are similar to the CNOP results produced using adjoint models. This indicates that the ensemble-based algorithm provides a practical method for extending the central concepts of CNOP to complex models. In this study, we pay attention to identifying the initial perturbations that are more likely to result in the onset of ENSO and develop into typical events, when starting from January. The CNOP approach is applied to the CESM model using the algorithm proposed by *Duan et al.* [2009]. The main objective is as follows.

The precursory disturbances for ENSO refer to the initial perturbations that develop into typical El Niño or La Niña events, which tend to onset in boreal spring and peak in late autumn or winter. To obtain the precursory disturbances, a number of initial sea temperature perturbations are superimposed during the neutral years, in which the absolute values of the Niño3 SST index are not greater than 0.5°C for 5 consecutive months; hence, no ENSO events exist. As such, 10 neutral years are selected, and the associated time series of the Niño3 SST index are shown in Figure 3. Each neutral year is integrated for 12 months beginning in January, with initial values being the initial sea temperature fields of the neutral year plus the initial perturbations. The initial perturbations are generated by taking the differences between the sea temperature in January of the neutral year and the temperatures in each of the 25 years before and after the neutral year. Thus, 50 different initial perturbations are obtained for each neutral year. However, an absolute Niño3 SST index value greater than 0.5°C may indicate that an ENSO event has begun. In this case, treating the corresponding initial perturbation as the precursory ENSO disturbance does not make sense. Therefore, among the 50 initial perturbations for each neutral year, only those with absolute Niño3 values smaller than 0.5°C are selected for the experiments. Table 1 lists the numbers of initial perturbations used in each neutral year. A total of 269 initial perturbations were used for the 10 neutral years.

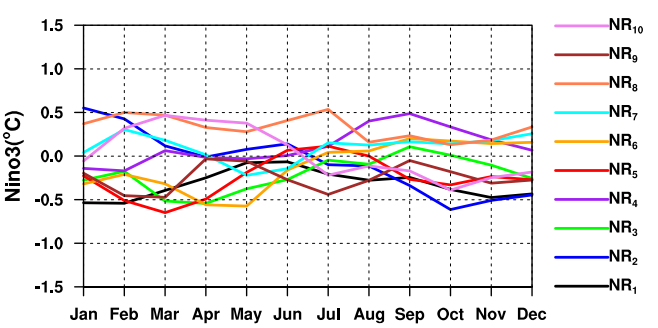

Figure 3. Time-dependent Niño3 indices of the 10 neutral years from the 100 year control run, denoted by NR_i (i = 1,. . . 10). In each year, Niño3 is generally smaller than 0.5°C and no ENSO events occur.

The 269 initial perturbations of sea temperature cover the tropical Pacific region (20.19°S–20.05°N, 130.44°E–84.49°W), extending from the surface to 165 m depth, which is approximately the bottom of the thermocline

Table 1. The Numbers of Initial Perturbations Superimposed During Each Neutral Year and the Numbers of Perturbations That Evolve Into El Niño and La Niña Events[a]

	NR_1	NR_2	NR_3	NR_4	NR_5	NR_6	NR_7	NR_8	NR_9	NR_{10}	total
Perturbations	27	36	21	25	23	24	25	30	23	35	269
El Niño	6	18	1	11	6	2	1	5	0	31	81
La Niña	6	1	12	1	0	6	7	15	14	0	62

[a]NR_i (i = 1, . . . 10) denotes the 10 neutral years. There are 269 initial perturbations for the 10 neutral years. Eighty-one evolve into El Niño events and 62 evolve into La Niña events.

over the western equatorial Pacific. As mentioned, a 12 month integration is performed for each initial perturbation to determine if an initial perturbation evolves into an El Niño or a La Niña event. We then identify the precursory disturbance that is most likely to evolve into an ENSO event. In this case, the resultant precursory disturbance is CNOP, which acts as the optimal precursory disturbance for ENSO. We examine two indices, denoted as T-Niño3 and F-Niño3. The indices represent monthly SST anomalies averaged over 5°N–5°S and 150°W–90°W. The former SST anomaly is computed relative to mean climatological values from the 100 year control run. The latter SSTA is calculated relative to each neutral year. El Niño (or La Niña) events are thought to occur when both T-Niño3 and F-Niño3 of an integration are greater than 0.5°C (or smaller than −0.5°C) for more than 5 consecutive months. Furthermore, if both indices peak in late autumn or winter, then the corresponding initial perturbation is deemed a precursory disturbance for warm or cold ENSO events. According to the definition of CNOP, an initial perturbation can serve as the optimal precursory disturbance for a climate event if and only if it exhibits the largest nonlinear growth. In this context, the precursory disturbance that produces the strongest ENSO event may represent the optimal precursory disturbance for an El Niño/La Niña event. In the following section, we explore the characteristics of precursory disturbances for El Niño and La Niña events using the CESM model and attempt to identify the optimal precursors.

4. The Precursory Disturbances for El Niño and La Niña Events

According to the methodology described above, we analyzed 269 initial perturbations from 10 neutral years and identified 81 precursory disturbances for El Niño events and 62 precursors for La Niña events (Table 1). The corresponding time-dependent T-Niño3 and F-Niño3 indices are shown in Figure 4. Both indices are greater than 0.5°C (and smaller than −0.5°C) for more than 5 months. Additionally, their peak values generally appear at the end of the year, indicating the occurrence of typical El Niño (and La Niña) events. To explore the spatial characteristics of these precursory disturbances, we conduct a combined empirical orthogonal function (CEOF) analysis. The leading CEOF represents 23.0% (and 34.0%) of the total variance for the precursory disturbances of El Niño (and La Niña). The time series PC1 indicates that some precursory disturbances for El Niño (and La Niña) exhibit spatial patterns similar to those of CEOF1, while others are opposite to those of CEOF1. In this sense, the precursory disturbances for El Niño and La Niña can be classified into two groups according to the sign of PC1. Members of the first group exhibit positive PC1 values, while members of the other group correspond to negative PC1 values. Specifically, of the 81 precursory disturbances of El Niño, we classify 37 precursory disturbances in the positive group and 44 in the negative group. Similarly, the 62 precursory disturbances of La Niña are classified into 33 positive disturbances and 29 negative disturbances. Then, a composite analysis was used to obtain two types of composite patterns associated with the precursory disturbances for El Niño and La Niña, including SSTAs and subsurface temperature anomalies in the equatorial Pacific (Figures 5 and 6). For El Niño, one type of precursory disturbances possesses a wide range of positive SST anomalies over the equatorial Pacific. In addition, the subsurface temperature component exhibits positive anomalies in the upper layers of the eastern equatorial Pacific and negative anomalies in the lower layers of the western equatorial Pacific (Figure 5a; hereafter referred to as an E-type1 precursory disturbance for El Niño). The other type of precursory disturbance consists of an SSTA component with negative anomalies in the central-eastern equatorial Pacific, negative subsurface temperature anomalies in the upper layers of the eastern equatorial Pacific and positive anomalies in the lower layers of the western equatorial Pacific (Figure 5b; hereafter referred to as an E-type2 precursory disturbance for El Niño). Regarding the two types of precursory disturbances for La Niña, their spatial structures

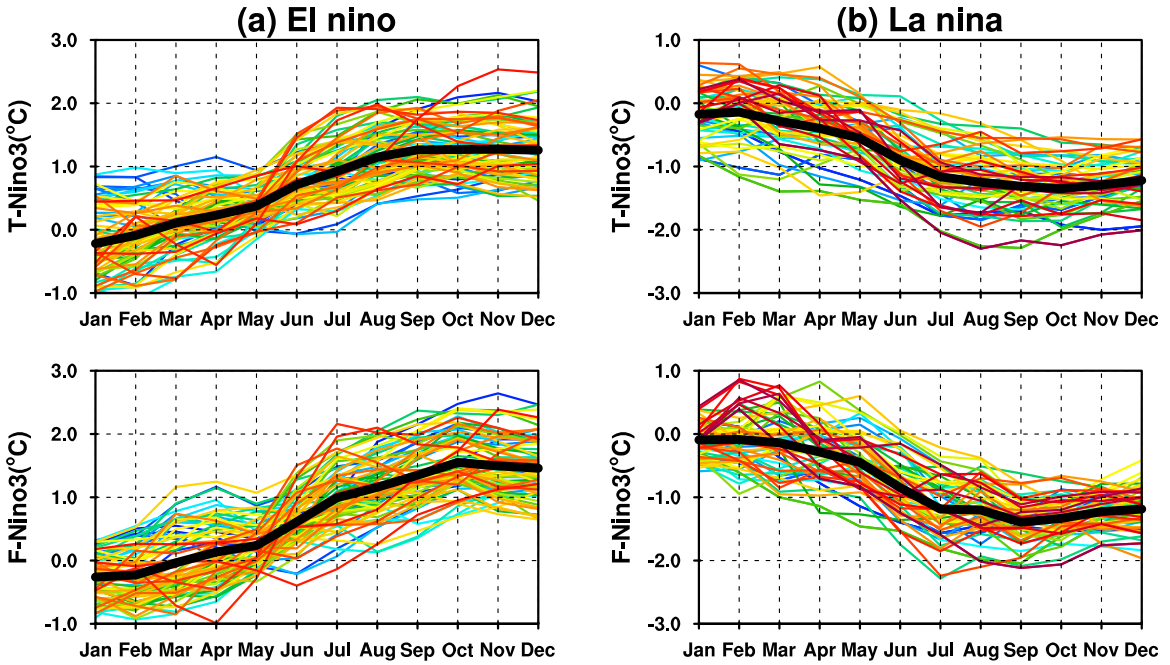

Figure 4. Time-dependent T-Niño3 and F-Niño3 indices of the 81 integrations for (a) El Niño and the 62 integrations for (b) La Niña events. The thick black lines are the ensemble means of individual indices.

are similar to the E-type1 and E-type2 precursory disturbances of El Niño, but with opposite signs. These disturbances are denoted as L-type1 and L-type2 (Figure 6).

The evolutionary mechanisms of precursory disturbances are addressed by tracking the time-dependent evolutions of SSTAs, sea surface wind anomalies and subsurface temperature anomalies caused by the initial precursory perturbations. The neutral year is subtracted from the aforementioned 12 month integrations to obtain the evolution of each initial perturbation. Figure 7 plots the composite evolutions of the SSTA, sea surface wind anomaly and subsurface temperature anomaly components of the E-type1 and E-type2 precursory disturbances for El Niño. The L-type1 and L-type2 precursory disturbances for La Niña are presented in Figure 8. Both the E-type1 and E-type2 precursory disturbances evolve into typical El Niño events, and

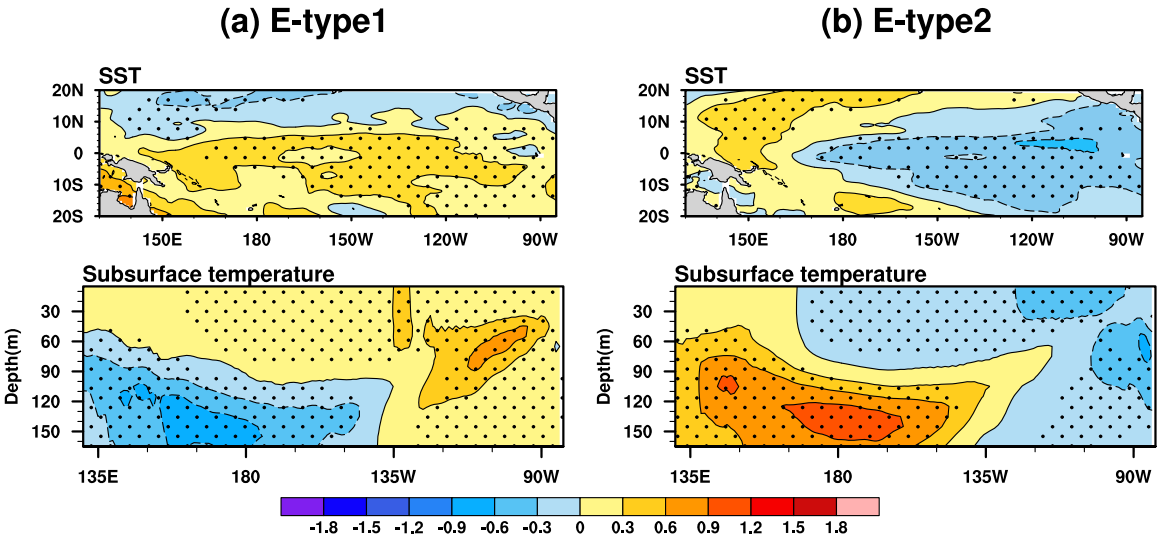

Figure 5. Composite two types of precursory disturbances for El Niño events, denoted as (a) E-type1 and (b) E-type2. Top plots show the SSTA component, while lower panels show the equatorial (5°S–5°N) subsurface temperature anomaly (units: °C). Dotted areas indicate that the composites exceed the 95% significance level, as determined by a *t* test.

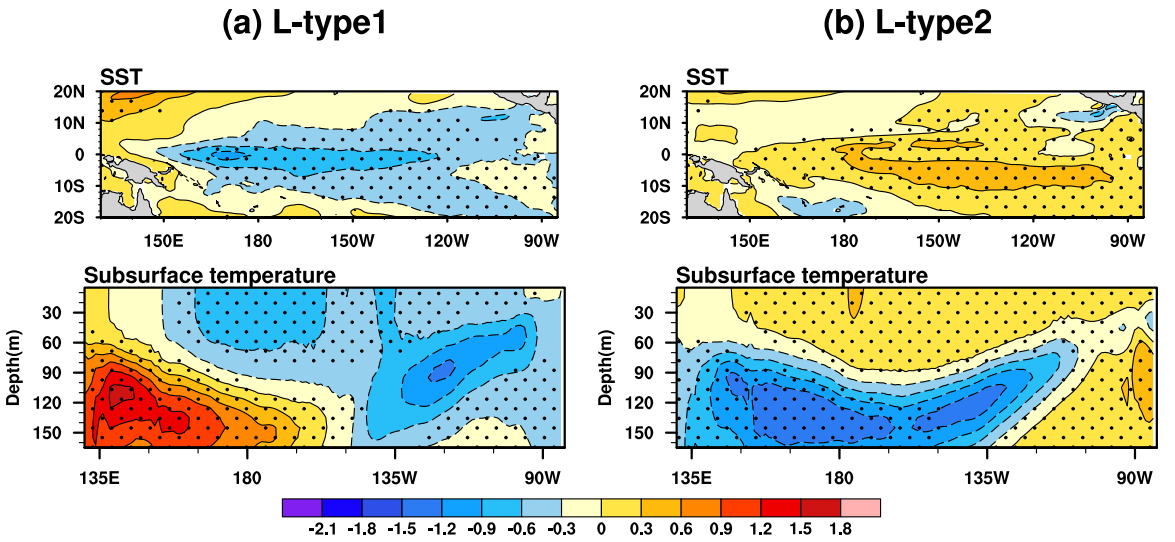

Figure 6. Same as Figure 5, but for precursory disturbances of La Niña events, denoted as (a) L-type1 and (b) L-type2.

both the L-type1 and L-type2 disturbances evolve into typical La Niña events. Specifically, in the case of the E-type2 and L-type2 precursory disturbances, the eastward propagation of the initial subsurface temperature anomalies in the western equatorial Pacific and the subsequent expansion to the sea surface in the

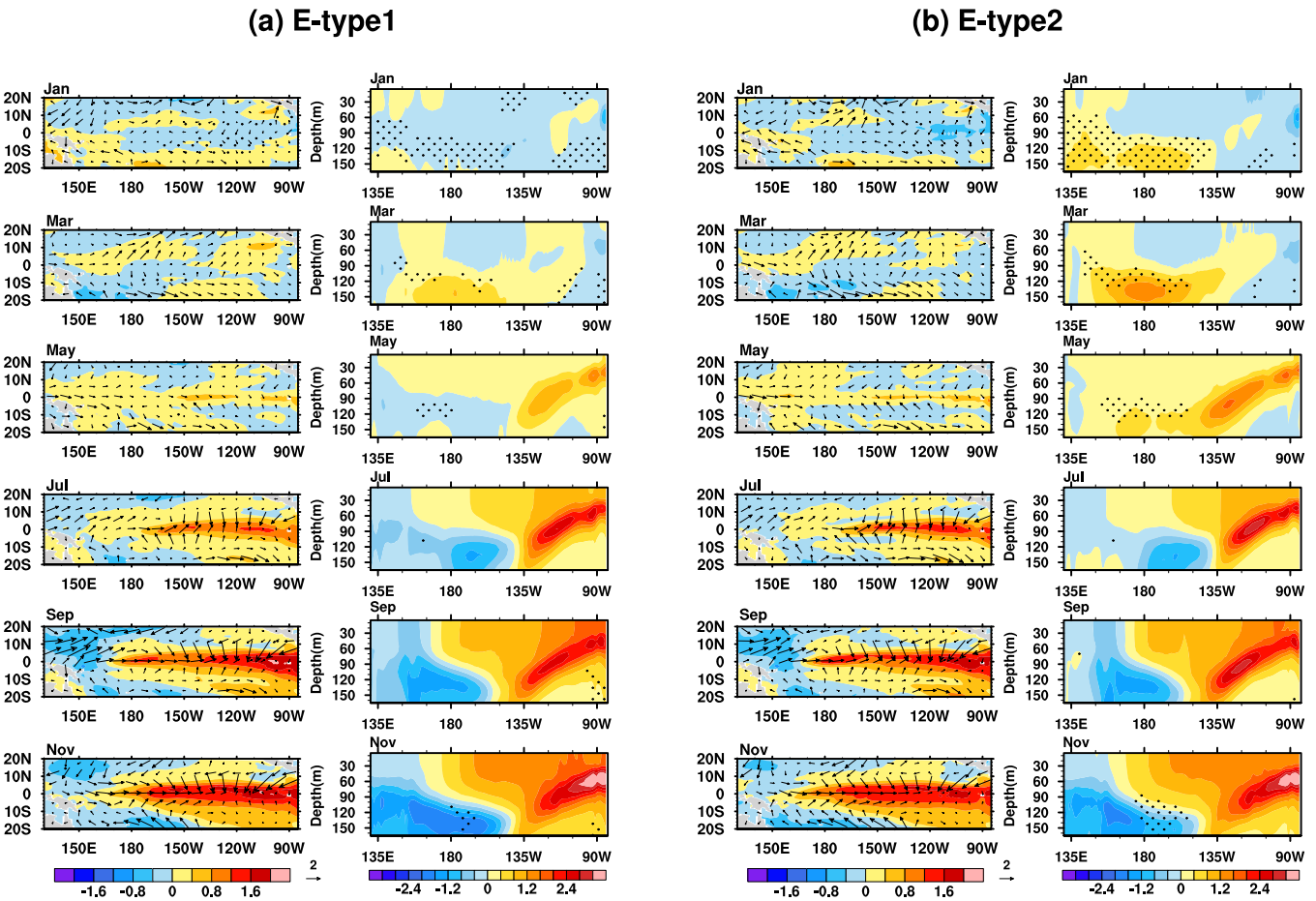

Figure 7. Composite evolutions of SSTAs (units: °C) and sea surface wind anomalies (units: m/s) over the tropical Pacific Ocean as well as equatorial (5°S–5°N) subsurface temperature anomalies (units: °C) for (a) E-type1 and (b) E-type2 precursory disturbances of El Niño. Dotted areas indicate that the composites exceed the 90% significance level, as determined by a *t* test.

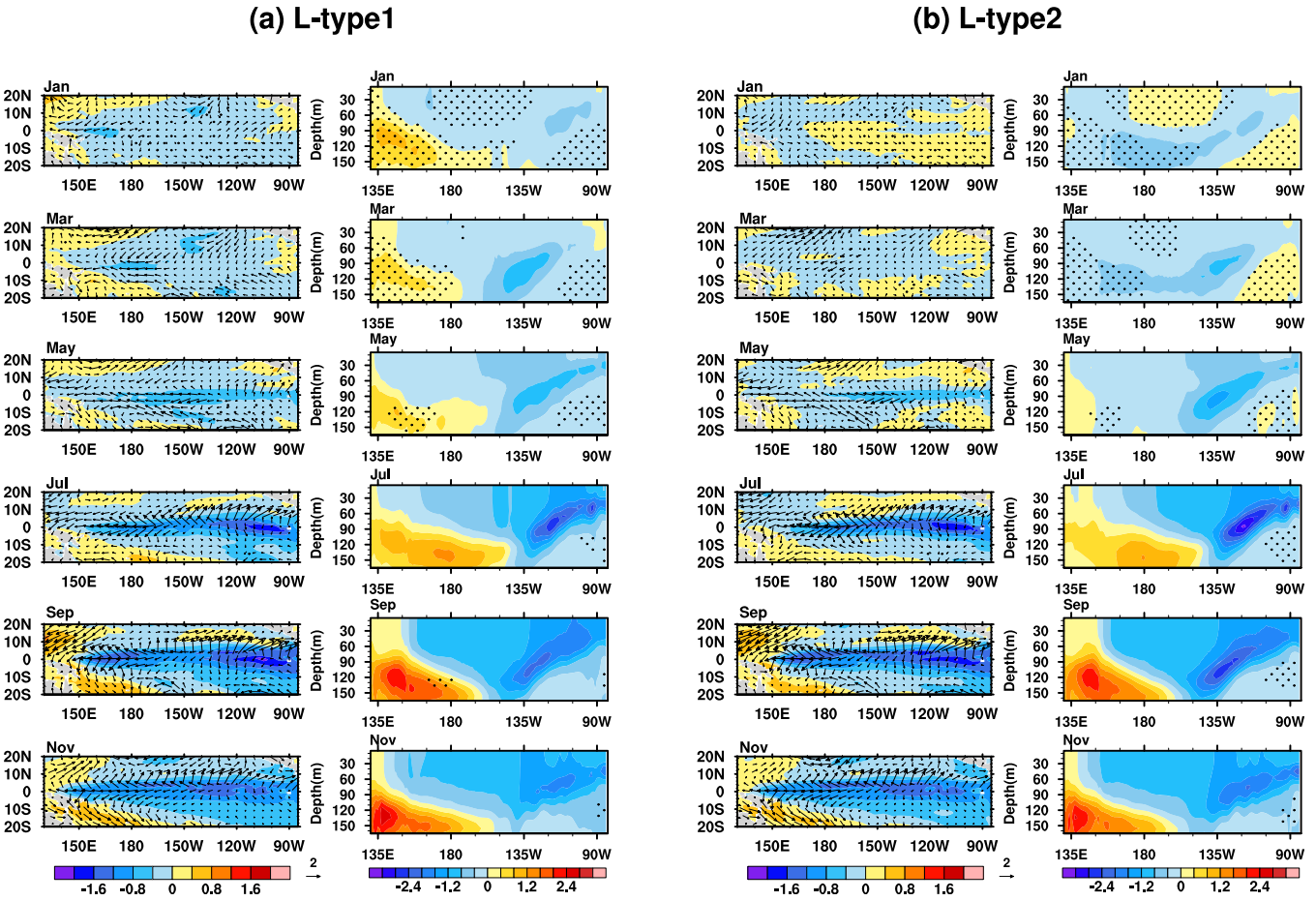

Figure 8. Same as Figure 7, but for the (a) L-type1 and (b) L-type2 precursory disturbances of La Niña.

eastern equatorial Pacific result in ENSO events. The initial positive (negative) subsurface temperature anomalies increase (decrease) the depth of the thermocline in the western Pacific and induce a downwelling (upwelling) Kelvin wave that travels eastward to increase (decrease) the thermocline depth in the eastern Pacific. This process favors the upward entrainment of warm (cold) subsurface water and the subsequent emergence of a positive (negative) SSTA. The warm (cold) SSTA in the Niño3 region is then amplified continuously by Bjerknes' positive feedback [*Bjerknes*, 1969], ultimately resulting in the development of El Niño (La Niña) events. For the E-type1 precursory disturbance, the initial patterns of sea temperature anomalies in the tropical Pacific are not persistent after 1 month (i.e., "Jan" in Figure 7a). One month later, positive sea temperature anomalies gradually reappear in the subsurface layers of the western equatorial Pacific, possibly due to the atmospheric westerly anomalies. Subsequently, these anomalies exhibit growth behaviors similar to those of E-type1. Thus, the evolution of the E-type2 precursory disturbance can be used to more effectively track the evolution of El Niño events compared to the evolution of the E-type1 disturbance. Additionally, E-type2 displays a much earlier signal associated with the occurrence of El Niño. Unlike the E-type1 precursory disturbance, the initial negative sea temperature anomalies in the upper layers of the eastern equatorial Pacific for L-type1 are maintained throughout the year. These anomalies constantly grow due to the upwelling of cold subsurface water and Bjerknes' positive feedback between SSTAs and zonal wind anomalies [*Bjerknes*, 1969]. Nevertheless, comparing the L-type1 and L-type2 precursory disturbances, the evolution of L-type1 is similar to the late phase evolution of L-type2, particularly after May (Figure 8b). Similarly, the precursory disturbance associated with the L-type2 spatial structure also exhibits a much earlier signal for the occurrence of La Niña events, favoring prediction of La Niña events with a longer lead time compared to the L-type1 precursory disturbance. However, do the E-type2 and L-type2 precursory disturbances represent the optimal precursory disturbances for El Niño and La Niña events, respectively?

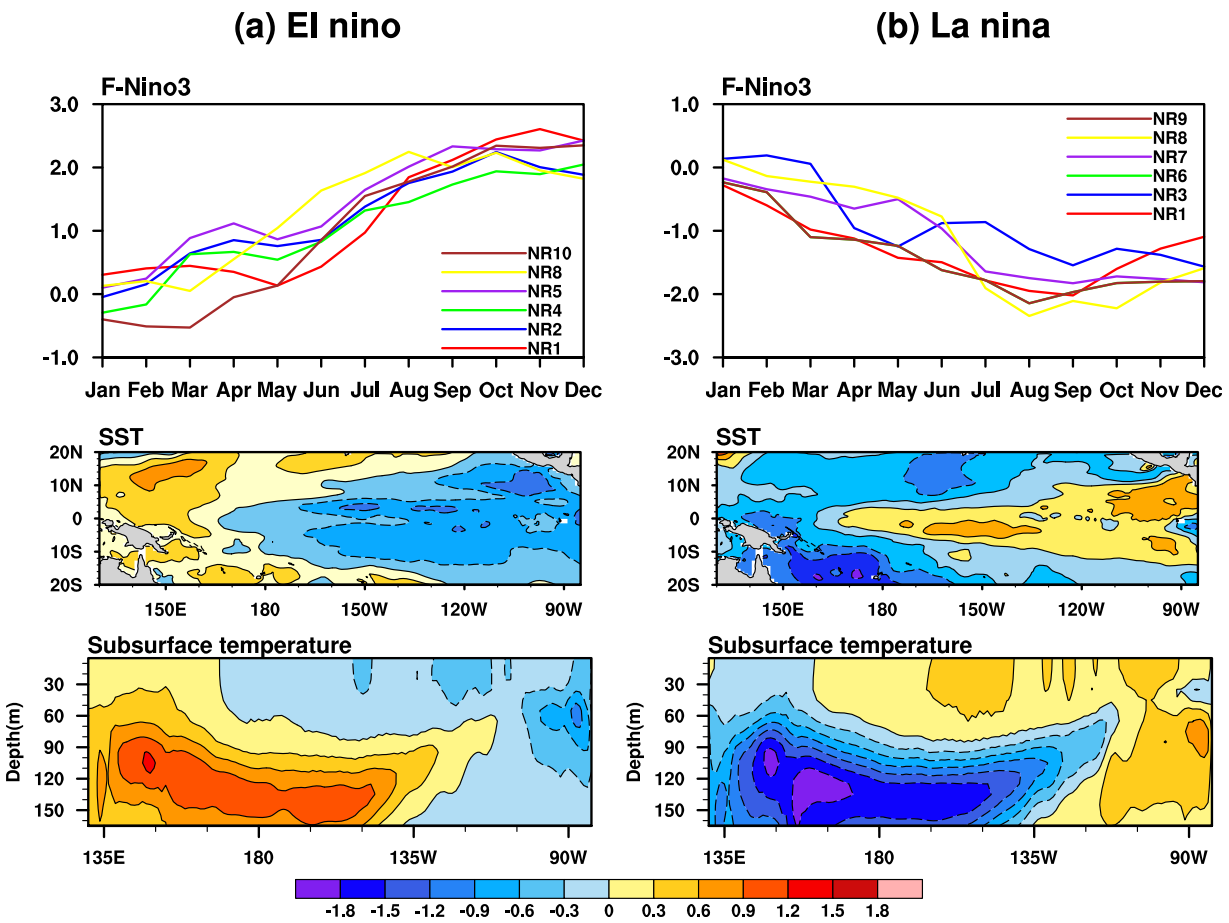

Figure 9. The F-Niño3 indices, composite SSTAs and subsurface temperature anomalies of six precursory disturbances for (a) El Niño and (b) La Niña. These six precursory disturbances induce the strongest El Niño/La Niña events in the corresponding neutral years. The remaining 4 neutral years are not considered because few precursory disturbances occurred and the associated ENSO events were weak.

As stated earlier, the optimal precursory disturbance for a climate event refers to the initial perturbation that is most likely to evolve into the climate event. CNOP is the initial perturbation that has the largest nonlinear growth during a prediction period and can act as the optimal precursor for a climate event [*Mu et al.*, 2003]. In terms of ENSO, the initial perturbation that induces the strongest ENSO event may represent the optimal precursory disturbance for an El Niño/La Niña event. Therefore, among the precursory disturbances identified above, we further explore those that exhibit the largest peak values of F-Niño3 (and T-Niño3). For different neutral years, the precursory disturbances with the largest peak values of F-Niño3 share similar spatial structures for both El Niño and La Niña. Figure 9 illustrates the composite of these precursory disturbances for El Niño and La Niña as well as the resultant F-Niño3 time series. Six precursory disturbances in the related neutral years are used in this composite analysis because few precursory disturbances occurred in the remaining 4 years and those disturbances were associated with weaker El Niño/La Niña events (see Table 1). The composite SST and subsurface temperature anomalies exhibit spatial patterns similar those of the E-type2 and L-type2 precursory disturbances shown in Figures 5b and 6b. In addition, these anomalies also grow in a manner similar to the growth behaviors of the E-type2 and L-type2 precursory disturbances (Figure 10). Thus, the initial perturbations with spatial characteristics of E-type2 and L-type2 precursory disturbances are more likely to develop into El Niño and La Niña events. In addition, these disturbances generally induce stronger ENSO events. Therefore, we consider the E-type2 and L-type2 precursory disturbances to be the optimal precursory disturbances for El Niño and La Niña events, respectively.

Figure 9 illustrates that the El Niño events are generally stronger than the La Niña events, which is often referred to as El Niño-La Niña amplitude asymmetry [*An and Jin*, 2004; *Im et al.*, 2015]. *An and Jin* [2004] and

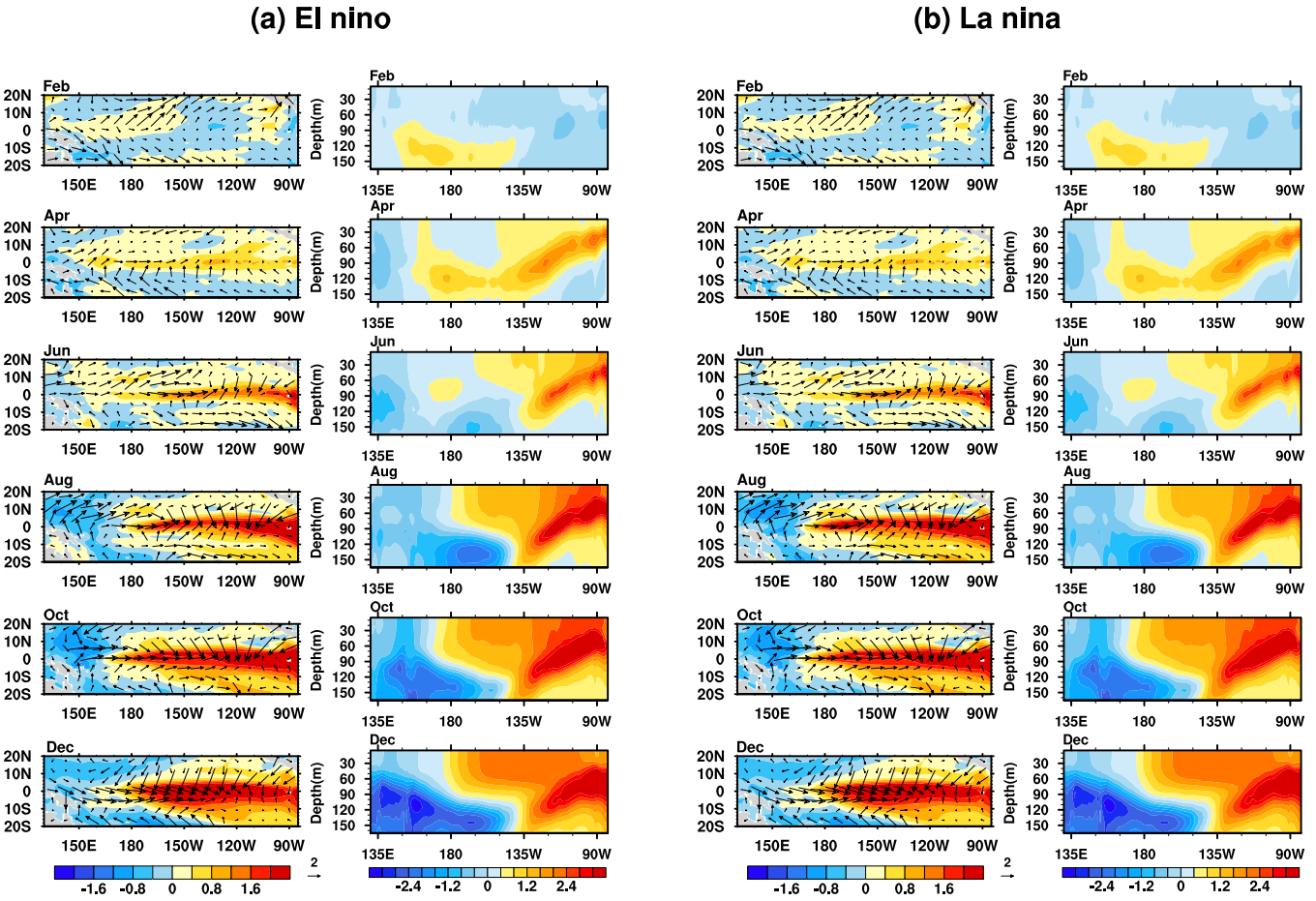

Figure 10. Composite evolutions of SSTAs (units: °C) and sea surface wind anomalies (units: m/s) over the tropical Pacific Ocean as well as the equatorial (5°S–5°N) subsurface temperature anomalies (units: °C) for the (a) El Niño and (b) La Niña precursory disturbances in Figure 9.

Duan and Mu [2006] suggested that nonlinearity is responsible for the amplitude asymmetry of ENSO, particularly the dynamic heating due to nonlinear temperature advection, which enhances El Niño and suppresses La Niña. CNOP can potentially resolve this issue and identify the asymmetric characteristics of El Niño and La Niña, which cannot be sufficiently revealed by traditional linear methods [*Duan and Mu*, 2006]. Examination of Figure 9 shows that the SST tendencies induced by nonlinear temperature advection are positive for both El Niño and La Niña, as has been previously revealed using simple models [*Duan and Mu*, 2006]. Furthermore, we examine the subsurface temperature anomalies of realistic ENSO events using the Simple Ocean Data Assimilation product version 2.1.6 (SODA) from 1970 to 2008 [*Carton and Giese*, 2008] to verify the theoretical results of the CNOP approach. A composite analysis is conducted for the 1972–1973, 1976–1977, 1982–1983, 1986–1987, 1997–1998 and 2006–2007 El Niño events, and the 1973–1974, 1975–1976, 1984–1985, 1988–1989, 1999–2000 and 2007–2008 La Niña events, as shown in Figure 11. Prior to peaking during boreal winter, the typical subsurface temperature anomalies associated with El Niño/La Niña are well established in January in the western equatorial Pacific. This trend qualitatively agrees with the optimal precursory disturbances for El Niño and La Niña events obtained in our study. The subsurface temperature anomalies extend eastward over time and influence the overlying SST in the eastern Pacific, eventually inducing the occurrence of El Niño/La Niña events. *Meinen and McPhaden* [2000] and *McPhaden* [2003] have reported that these subsurface temperatures can improve ENSO predictions when used to produce initial subsurface conditions in the equatorial Pacific. The consistency between our results and observations suggests that CNOP is physically applicable within the CESM framework. The difference is that the CNOP can identify the optimal precursory disturbances that are more likely to evolve into stronger ENSO events.

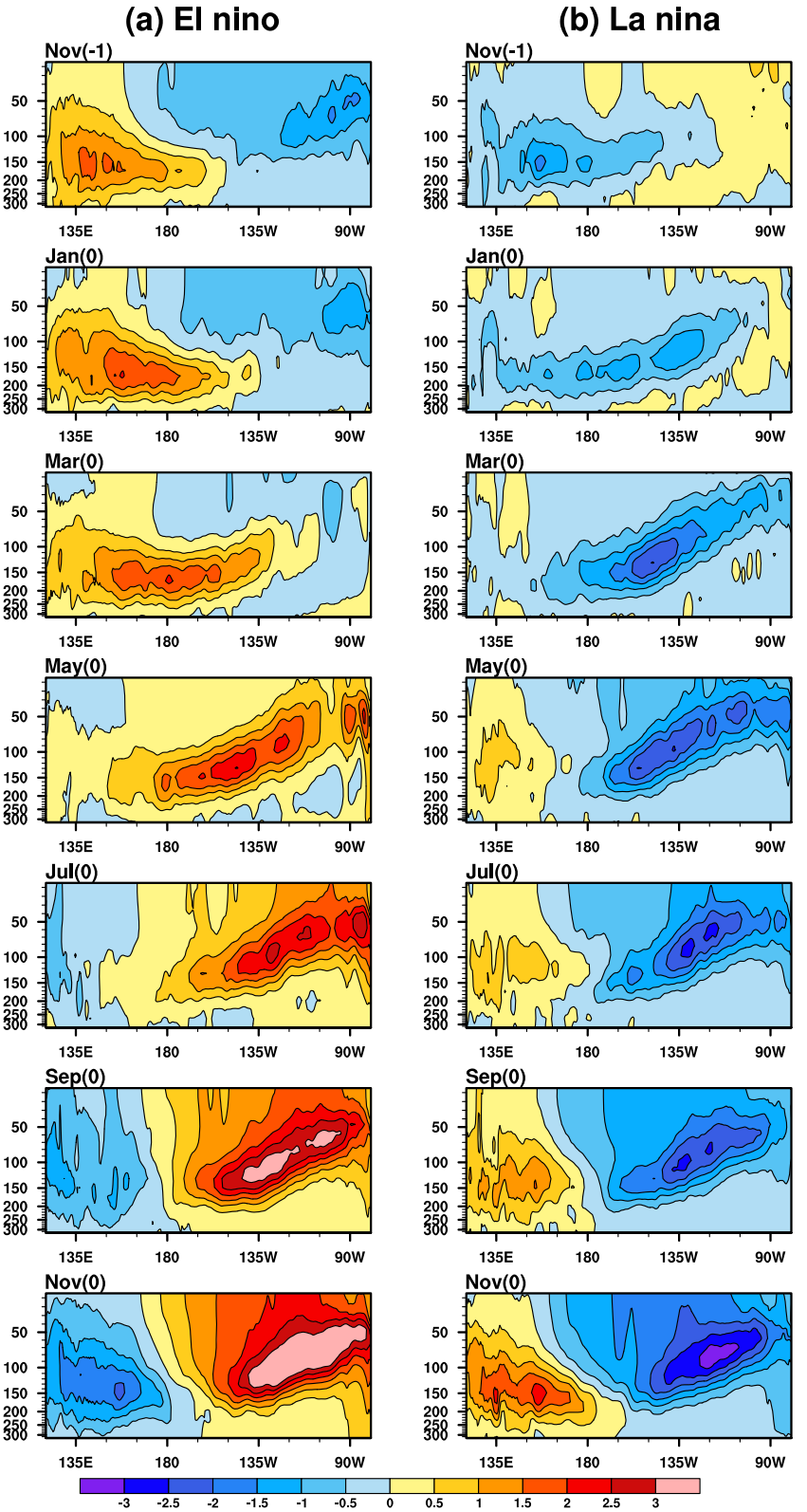

Figure 11. Composite evolution of the subsurface temperature anomalies along the equatorial Pacific (5°S–5°N) for observed (a) El Niño and (b) La Niña events. The composites span from November (−1) before the El Niño/La Niña year to November (0) of the El Niño/La Niña year.

5. Relationship Between Optimal Precursory Disturbances and OGEs Associated With ENSO and Implications to Target Observation

The "target observations" or "adaptive observations" strategies refer to processes in which additional observations are prioritized in specific localized areas to better predict an event. Additional observations in these specific areas, generally called "sensitive areas," are expected to have a large contribution to reduce the associated prediction errors. The determination of sensitive areas is a key problem in target observations [*Snyder*, 1996; *Mu*, 2013; *Mu et al*., 2015]. Additional observations in these sensitive areas are assimilated using a data assimilation system, providing a more reliable initial state for the model and a more accurate prediction. Target observations offer an economical and efficient way for improving predictions of weather and climate events. Due to the high costs of field observations over the ocean, focusing on "sensitive areas" may represent an economical and efficient strategy for improving the prediction of ENSO events. *Duan and Hu* [2015] identified two types of optimally growing initial errors (OGEs) for ENSO predictions using the CESM model, namely, type-1 and type-2 OGEs. They suggested that the sensitive areas are the lower layers of the western equatorial Pacific and the upper layers of the eastern equatorial Pacific. The elimination of initial errors in sensitive areas using target observations can greatly improve ENSO forecasting.

In section 4 of this study, we have demonstrated that two types of precursory disturbances exist for El Niño and La Niña events using the CESM model. E-type2 and L-type2 represent the optimal precursory disturbances for El Niño and La Niña events, respectively. However, what is the relationship between the optimal precursory disturbances for ENSO and the two types of OGEs obtained in *Duan and Hu* [2015]? The optimal precursory disturbances for El Niño and La Niña events, namely E-type2 and L-type2 in Figures 5b and 6b, exhibit structures that are similar to those of type-2 OGEs [see *Duan and Hu*, 2015, Figure 6b]. The similarities between the optimal precursory disturbances and the type-2 OGEs can be examined using the following similarity coefficient:

$$r=\frac{\langle T^{\alpha}\cdot T^{\beta}\rangle}{\|T^{\alpha}\|\|T^{\beta}\|}=\frac{\sum_{i=1}^{m}\sum_{j=1}^{n}T_{ij}^{\alpha}T_{ij}^{\beta}}{\sqrt{\sum_{i=1}^{m}\sum_{j=1}^{n}\left(T_{ij}^{\alpha}\right)^{2}\sum_{i=1}^{m}\sum_{j=1}^{n}\left(T_{ij}^{\beta}\right)^{2}}} \tag{3}$$

where the optimal precursory disturbances and the OGE fields are assumed to be vectors $T^{\alpha}=(T_{ij}^{\alpha})_{m\times n}$ and $T^{\beta}=(T_{ij}^{\beta})_{m\times n}$, respectively. T_{ij}^{α} and T_{ij}^{β} represent the sea temperature values at different grids, and (i, j) are the grid points in the tropical Pacific. The results show that the optimal precursory disturbance for El Niño is negatively correlated with the type-2 OGEs, while that of La Niña is positively correlated with the type-2 OGEs. For the entire tropical Pacific ranging from 20°S to 20°N and from the surface to 165 m, the similarity index value between the optimal precursory disturbance for El Niño/La Niña, i.e., the E-type2/L-type2 precursory disturbance, and the type-2 OGEs is −0.62/0.62. If averaged over the area between 5°S and 5°N of the equatorial Pacific, a higher degree of similarity exists, with an index value of −0.90/0.94 between the E-type2/L-type2 precursory disturbance and the type-2 OGEs. In addition to the similar spatial patterns between the optimal precursory disturbance for El Niño/La Niña and the type-2 OGEs, the related error growth behavior associated with El Niño forecasting is similar to the growth behaviors of the E-type2 and L-type2 optimal precursory disturbances. In this study, we show that the occurrence and development of El Niño/La Niña is mainly dependent on the sea temperature anomalies in the areas associated with the subsurface layers of the western equatorial Pacific and the surface layers in the eastern equatorial Pacific, especially in the Niño3 region. These two key areas for ENSO development are the same sensitive areas for target observations determined by *Duan and Hu* [2015]. Therefore, combining the optimally growing initial errors and the optimal precursory disturbances for ENSO, we can infer that adding observations in sensitive areas and assimilating them into the initial field can not only decrease the initial errors but also better detect precursory signals of ENSO, which can greatly improve ENSO forecasting.

6. Conclusion and Discussion

This study uses the CESM model to reveal the precursory disturbances that develop into typical El Niño and La Niña events. Furthermore, the optimal precursory disturbances for El Niño and La Niña events are identified according to the definition of CNOP. Specifically, we examine the relationship between the optimal precursory disturbances and the optimally growing initial errors associated with ENSO prediction. Two types of

precursory disturbances exist for El Niño and La Niña events. In the case of El Niño, the E-type1 precursory disturbance exhibits a wide range of positive SST anomalies over the equatorial Pacific. In addition, the subsurface temperature component exhibits positive anomalies in the upper layers of the eastern equatorial Pacific and negative anomalies in the lower layers of the western equatorial Pacific. E-type2 consists of an SSTA component with negative anomalies in the central-eastern equatorial Pacific as well as negative subsurface temperature anomalies in the upper layers of the eastern equatorial Pacific and positive anomalies in the lower layers of the western equatorial Pacific. The two types of precursory disturbances associated with La Niña, L-type1 and L-type2, are opposed to those of El Niño.

The resultant SSTA in the Niño3 region generally occurs in the spring and peaks at the end of the year, indicating the occurrence of typical El Niño and La Niña events. For the E-type2 and L-type2 precursory disturbances, the initial anomaly signals in the subsurface layers of the western equatorial Pacific gradually propagate eastward and then grow in the equatorial eastern Pacific. The initial patterns of the E-type1 precursory disturbance are not persistent and evolve in a manner similar to the growth of E-type2 after 1 month. L-type1 exhibits a locally constant growth associated with temperature anomalies, which initially occur in the upper layers of the eastern equatorial Pacific. Compared with E-type1 and L-type1, the E-type2 and L-type2 precursory disturbances exhibit much earlier signals for El Niño and La Niña events. Furthermore, according to the definition of CNOP, we identify the precursory disturbances that are most likely to evolve into El Niño and La Niña events. These precursory disturbances are similar to the E-type2 and L-type2 precursory disturbances. Thus, the E-type2 and L-type2 precursory disturbances may represent the optimal precursory disturbances for El Niño and La Niña events, respectively. These theoretical results are qualitatively verified for the observed El Niño and La Niña events.

We found that the optimal precursory disturbances for El Niño and La Niña events are similar to the optimally growing initial errors associated with ENSO prediction. The related growth behaviors are also similar. The onset of an ENSO event caused by the optimal precursory disturbance is mainly attributed to sea temperature anomalies in the subsurface layers of the equatorial western Pacific and their subsequent growth in the surface layers of the eastern equatorial Pacific. The optimally growing initial errors indicate that these two areas represent sensitive areas of target observations associated with ENSO prediction. Therefore, combining the optimal precursory disturbances and the optimally growing initial errors for ENSO suggests that the observation network should be improved by target observations in sensitive areas. These improvements will benefit precursory signal detection, avoid false predictions and decrease initial errors in sensitive areas, thereby enhancing ENSO forecasting.

Duan et al. [2013] explored the optimal precursory disturbances for El Niño events using the CNOP approach in the Zebiak–Cane model. They observed a zonal SSTA dipole pattern with positive anomalies in the eastern equatorial Pacific and negative anomalies in the central equatorial Pacific as well as a deepening thermocline depth along the equatorial Pacific. Using the Zebiak–Cane model, *Mu et al*. [2014] further demonstrated that the optimally growing initial errors of El Niño predictions are similar to the optimal precursory disturbances for El Niño and La Niña events. This study used the CESM model to obtain the optimal precursory disturbances for El Niño and La Niña events, namely, E-type2 and L-type2 in Figures 5b and 6b. In addition, we illustrated the similarities between these precursors and the optimally growing initial errors. Unlike the simple Zebiak–Cane model, complex coupled models such as CESM do not include an oceanic variable associated with the thermocline depth anomaly. Nevertheless, a deepening thermocline depth along the equatorial Pacific generally suggests that warm subsurface water has accumulated in the equatorial Pacific, corresponding to the positive subsurface temperature anomalies. Accordingly, the results of this study were compared with those obtained using the Zebiak–Cane model. The optimal precursors in the Zebiak–Cane model mirror the patterns of the E-type1 and L-type1 precursory disturbances for El Niño and La Niña. Nevertheless, the above analysis revealed that the E-type2 and L-type2 precursory disturbances, compared to E-type1 and L-type1, present a much earlier signal associated with the occurrence of El Niño and La Niña. Additionally, these types are similar to the precursory disturbances identified by the definition of CNOP, representing the optimal precursory disturbances for ENSO events. Therefore, the optimal precursory disturbances obtained by the CESM model precede those obtained using the Zebiak–Cane model and are helpful for ENSO forecasting with much longer leading times.

In addition to the CESM model used in this study, ENSO behavior and relevant perturbation growth have been documented by the NCAR Community Climate System Model version 4 (CCSM4), the predecessor of

the CESM model. *Deser et al*. [2012] examined the seasonal evolutions of ENSO based on a 1300 year preindustrial control simulation using CCSM4. These evolutions can be explained mechanistically by the delayed oscillator and recharge/discharge oscillator, particularly for the linear aspects of El Niño and La Niña. With the same simulation data sets, *Dinezio and Deser* [2014] further illustrated that the nonlinearity of the delayed thermocline feedback is responsible for the multiyear persistence of La Niña, contributing to the asymmetrical durations of El Niño and La Niña. Combined with the results in this study, the precursory roles of the equatorial subsurface anomalies are highlighted by the ENSO variations. *Anderson and Perez* [2015] suggested that the subsurface anomalies across the equatorial Pacific may be forced by trade wind variations in the extratropical North Pacific due to a trade wind charging (TWC) mechanism rather than the ENSO cycle itself. However, it is beyond the scope of this study to identify the origins of initial precursory disturbances. In addition, *Larson and Kirtman* [2015] demonstrated that coupled instabilities alone can cause large growth of SST perturbations, in the absence of ENSO itself, subsurface precursors and large-scale atmospheric triggers. These results indicate that no specific precursors or triggers can solely determine the initiation and development of ENSO. Thus, the onset of ENSO is difficult to accurately predict.

In this study, the optimal precursory disturbances of ENSO were obtained using the CNOP approach by the ensemble-based method [*Mu et al*., 2003; *Duan et al*., 2009]. These disturbances were identified from an ensemble of initial perturbations generated by taking the sea temperature differences in the tropical Pacific between a particular month and the starting month. However, this strategy may not guarantee that the constructed initial perturbations encompass all kinds of initial patterns. Hence, the optimal precursory disturbances obtained in the present study may only approximate the theoretical disturbances. Therefore, a more effective algorithm must be developed to compute CNOP in complex models. In addition, we emphasize the role of sea temperature anomalies in the equatorial Pacific 1 year in advance in leading to occurrence of ENSO events. However, in addition to these anomalies, the onset of ENSO may also need to be triggered by atmospheric variations, such as westerly wind anomalies in the equatorial western Pacific [*Lengaine et al*., 2004; *Lian et al*., 2014]. ENSO precursors have also been shown to exist outside the tropical Pacific, including the SST and wind variations in the Indian Ocean [*Clarke and Van Gorder*, 2003; *Izumo et al*., 2014] and Atlantic Ocean [*Rodríguez-Fonseca et al*., 2009; *Dayan et al*., 2014] as well as in the subtropical Pacific, such as SST variations described by the Pacific Meridional Mode [*Chang et al*., 2007; *Larson and Kirtman*, 2013, 2014]. These results suggest that combining different factors may improve the predictabilities of both the El Niño and La Niña onsets.

Furthermore, in addition to the traditional "Eastern Pacific El Niño" (EP-El Niño) events examined in this study, "Central Pacific El Niño" (CP-El Niño) events have become more frequent and common during the late twentieth century, especially after the 1990s [*Ashok et al*., 2007; *Kao and Yu*, 2009; *Kug et al*., 2009]. The evolution of CP-El Niño events is mainly due to zonal advective feedback rather than thermocline feedback. Consequently, what are the characteristics of optimal precursory disturbances for CP-El Niño events? Additionally, what, if any, relationship exists between these events and EP-El Niño events? Such questions must be answered in future studies.

Acknowledgments.
The authors are grateful for the useful comments provided by the two anonymous reviewers. This work was jointly sponsored the National Natural Science Foundation of China (grants 41525017 and 41230420) and the National Programme on Global Change and Air-Sea Interaction grant GASI-IPOVAI-06. The ERSST V3 data used in this study are available at http://www.ncdc.noaa.gov/data-access/. The SODA data can be obtained from http://soda.tamu.edu/data.htm.

References

AchutaRao, K., and K. R. Sperber (2002), Simulation of the El Niño Southern Oscillation: Results from the Coupled Model Intercomparsion Project, *Clim. Dyn.*, *19*, 191–209.
An, S.-I., and F.-F. Jin (2004), Nonlinearity and asymmetry of ENSO, *J. Clim.*, *17*, 2399–2412.
An, S.-I., and B. Wang (2001), Mechanisms of locking the El Niño and La Niña mature phases to boreal winter, *J. Clim.*, *14*, 2164–2176.
Anderson, B. T., and R. C. Perez (2015), ENSO and non-ENSO induced charging and discharging of the equatorial Pacific, *Clim. Dyn.*, *45*(9), 1–19, doi:10.1007/s00382-015-2472-x.
Ashok, K., S. Behera, S. A. Rao, H. Weng, and T. Yamagata (2007), El Niño Modoki and its possible teleconnection, *J. Geophys. Res.*, *112*, C11007, doi:10.1029/2006JC003798.
Birgin, E. G., J. M. Marínez, and M. Raydan (2000), Nonmonotone spectral projected gradient methods on convex sets, *SIAM J. Optim.*, *10*, 1196–1211.
Bjerknes, J. (1969), Atmospheric teleconnections from the equatorial pacific, *Mon. Weather Rev.*, *97*(3), 163–172.
Carton, J. A., and B. S. Giese (2008), A reanalysis of ocean climate using simple ocean data assimilation (SODA), *Mon. Weather. Rev.*, *146*, 2999–3017.
Chang, P., L. Zhang, R. Saravanan, D. J. Vimont, J.C.H. Chiang, L. Ji, H. Seidel, and M. K. Tippett (2007), Pacific meridional mode and El Niño-Southern Oscillation, *Geophys. Res. Lett.*, *34*, L16608, doi:10.1029/2007GL030302.
Chen, D., and M. A. Cane (2008), El Niño prediction and predictability, *J. Comput. Phys.*, *227*(7), 3625–3640, doi:10.1016/j.jcp.2007.05.014.
Chen, D., M. A. Cane, A. Kaplan, S. E. Zebiak, and D. J. Huang (2004), Predictability of El Niño over the past 148 years, *Nature*, *428*(6984), 733–736.

Clarke, A. J., and S. Van Gorder (2003), Improving El Niño prediction using a space-time integration of Indo-Pacific winds and equatorial Pacific upper ocean heat content, *Geophys. Res. Lett.*, *30*(7), 1399, doi:10.1029/2002GL016673.
Craig, A. P., M. Vertenstein, and R. Jacob (2012), A new flexible coupler for earth system modeling developed for CCSM4 and CESM1, *Int. J. High Performance Comput. Appl.*, *26*(1), 31–42, doi:10.1177/1094342011428141.
Dayan, H., J. Vialard, T. Iaumo, and M. Lengaigne (2014), Does sea surface temperature outside the tropical Pacific contribute to enhanced ENSO predictability?, *Clim. Dyn.*, *43*, 1311–1325.
Deser, C., et al. (2012), ENSO and Pacific Decadal Variability in the Community Climate System Model Version 4, *J. Clim.*, *25*, 2622–2651.
Dinezio, P. N., and C. Deser (2014), Nonlinear Controls on the Persistence of La niña, *J. Clim.*, *27*, 7335–7355.
Duan, W. S., and J. Y. Hu (2015), The initial errors that induce a significant "spring predictability barrier" for El Niño events and their implications for target observation: Results from an earth system model, *Clim. Dyn.*, doi:10.1007/s00382-015-2789-5, in press.
Duan, W. S., and M. Mu (2006), Investigating decadal variability of El Niño Southern Oscillation asymmetry by conditional nonlinear optimal perturbation, *J Geophys. Res.*, *111*, C07015, doi:10.1029/2005JC003458.
Duan, W. S., and M. Mu (2009), Conditional nonlinear optimal perturbation: Applications to stability, sensitivity, and predictability, *Sci. China Ser. D*, *52*(7), 883–906.
Duan, W. S., M. Mu, and B. Wang (2004), Conditional nonlinear optimal perturbations as the optimal precursors for El Niño–Southern Oscillation events, *J. Geophys. Res.*, *109*, D23105, doi:10.1029/2004JD004756.
Duan, W. S., X. C. Liu, K. Y. Zhu, and M. Mu (2009), Exploring the initial errors that cause a significant "spring predictability barrier" for El Niño events, *J. Geophys. Res.*, *114*, C04022, doi:10.1029/2008JC004925.
Duan, W. S., Y. S. Yu, H. Xu, and P. Zhao (2013), Behaviors of nonlinearities modulating the El Niño events induced by optimal precursory disturbances, *Clim. Dyn.*, *40*, 1399–1413, doi:10.1007/s00382-012-1557-z.
Hunke, E. C., and W. H. Lipscomb (2008), CICE: The Los Alamos sea ice model, documentation and software, version 4.0, *Tech. Rep. LA-CC-06-012*, 76 pp., Los Alamos Natl. Lab., Los Alamos, N. M. [Available at http://climate.lanl.gov/Models/CICE/index.htm.]
Hurrell, J. W., et al. (2013), The Community Earth System Model: A framework for collaborative research, *Bull. Am. Meteorol. Soc.*, *94*(9), 1339–1360, doi:10.1175/BAMS-D-12-001211.
Im, S.-H., S.-I. An, S. T. Kim, and F.-F. Jin (2015), Feedback processes responsible for El Niño-La Niña amplitude asymmetry, *Geophys. Res. Lett.*, *42*, 5556–5563, doi:10.1002/2015GL064853.
Izumo, T., M. Lengaigne, J. Vialard, J. J. Luo, Y. Yamagata, and G. Madec (2014), Influence of Indian Ocean Dipole and Pacific Recharge on Following year's El Niño: Interdecadal robustness, *Clim. Dyn.*, *42*(1–2), 291–310.
Jin, E. K., et al. (2008), Current status of ENSO prediction skill in coupled ocean-atmosphere models, *Clim. Dyn.*, *31*(6), 647–664.
Kao, H. Y., and J. Y. Yu (2009), Contrasting eastern-Pacific and central-Pacific types of ENSO, *J. Clim.*, *22*(3), 615–632.
Kirtman, B. P., J. Shukla, M. Balmaseda, N. Graham, C. Penland, Y. Xue, and S. Zebiak (2002), Current status of ENSO forecast skill: A report to the Climate Variability and Predictability (CLIVAR) Working Group on seasonal to interannual prediction, International CLIVAR Project Office Rep. 56, 24 pp.
Kug, J. S., F. F. Jin, and S.-I. An (2009), Two types of El Niño events: Cold tongue El Niño and warm pool El Niño, *J. Clim.*, *22*(6), 1499–1515.
Larson, S., and B. Kirtman (2013), The Pacific Meridional Mode as a trigger for ENSO in a high-resolution coupled model, *Geophys. Res. Lett.*, *40*, 3189–3194, doi:10.1002/grl.50571.
Larson, S. M., and B. P. Kirtman (2014), The Pacific Meridional Mode as an ENSO Precursor and Predictor in the North American Multimodel Ensemble, *J. Clim.*, *27*, 7018–7032, doi:10.1175/JCLI-D-14-00055.1.
Larson, S. M., and B. P. Kirtman (2015), Revisiting ENSO Coupled Instability Theory and SST Error growth in a fully coupled model, *J. Clim.*, *28*, 4724–4742.
Lengaine, M., E. Guilyardi, J. P. Boulanger, C. Menkes, P. Delecluse, P. Inness, J. Cole, and J. Slingo (2004), Triggering of El Niño by westerly wind events in a coupled general circulation model, *Clim. Dyn.*, *23*(6), 601–620, doi:10.1007/s00382-004-0457-2.
Lian, T., D. Chen, Y. Tang, and Q. Wu (2014), Effects of westerly wind bursts on El Niño: A new perspective, *Geophys. Res. Lett.*, *41*, 3522–3527, doi:10.1002/2014GL059989.
Lipscomb, W. H., J. G. Fyke, M. Vizcaino, W. J. Sacks, J. Wolfe, M. Vertenstein, A. Craig, E. Kluzek, and D. M. Lawrence (2013), Implementation and initial evaluation of the Glimmer Community Ice Sheet Model in the Community Earth System Model, *J. Clim.*, *26*(19), 7352–7371.
Lopez, H., and K. P. Kirtman (2014), WWBs, ENSO predictability, the spring barrier and extreme events, *J. Geophys. Res. Atmos.*, *119*, 10,114–10,138, doi:10.1002/2014JD021908.
McPhaden, M. J. (2003), Tropical Pacific Ocean heat content variations and ENSO persistence barriers, *Geophys. Res. Lett.*, *30*(9), 1480, doi:10.1029/2003GL016872.
Meinen, C. S., and M. J. McPhaden (2000), Observations of warm water volume changes in the equatorial Pacific and their relationship to El Niño and La Niña, *J. Clim.*, *13*(20), 3551–3559.
Moore, A. M., and R. Kleeman (1996), The dynamics of error growth and predictability in a coupled model of ENSO, *Q. J. R. Meteorol. Soc.*, *122*, 1405–1446.
Mu, M. (2013), Methods, current status, and prospect of targeted observation, *Sci. China Earth Sci.*, *56*(12), 1997–2005.
Mu, M., W. S. Duan, and B. Wang (2003), Conditional nonlinear optimal perturbation and its applications, *Nonlinear Process Geophys.*, *10*(6), 493–501.
Mu, M., W. S. Duan, and B. Wang (2007a), Season-dependent dynamics of nonlinear optimal error growth and El Niño–Southern Oscillation predictability in a theoretical model, *J. Geophys. Res.*, *112*, D10113, doi:10.1029/2005JD006981.
Mu, M., H. Xu, and W. S. Duan (2007b), A kind of initial errors related to "spring predictability barrier" for El Niño events in Zebiak-Cane model, *Geophys. Res. Lett.*, *34*, L03079, doi:10.1029/2006GL027412.
Mu, M., W. S. Duan, D. Chen, and W. Yu (2015), Target observations for improving initialization of high-impact ocean-atmospheric environmental events forecasting, *Natl. Sci. Rev.*, *2*, 226–236, doi:10.1093/nsr/nwv021.
Mu, M. Q., and C. Y. Li (2000), Interactions between subsurface ocean temperature anomalies in the Western Pacific Warm Pool and ENSO cycle, *Chin. J. Atmos. Sci.*, *24*(4), 447–460.
Neale, R. B., J. Richter, S. Park, P. H. Lauritzen, S. J. Vavrus, P. J. Rasch, and M. Zhang (2013), The Mean Climate of the Community Atmosphere Model (CAM4) in forced SST and fully coupled experiments, *J. Clim.*, *26*(14), 5150–5168.
Mu, M., Y. S. Yu, H. Xu, and T. T. Gong (2014), Similarities between optimal precursors for ENSO events and optimally growing initial errors in El Niþo predictions, *Theor. Appl. Climatol.*, *115*, 461–469.
Newman, M., M. A. Alexander, and J. D. Scott (2011), An empirical model of tropical ocean dynamics, *Clim. Dyn.*, *37*, 1823–1841, doi:10.1007/s00382-011-1034-0.

Oleson, K. W., et al. (2010), Technical description of version 4.0 of the Community Land Model (CLM), *NCAR Tech. Note NCAR/TN-478+STR*, 257 pp., Natl. Cent. for Atmos. Res., Boulder, Colo.
Palmer, T. N., R. Buizza, F. Molteni, Y. C. Chen, and S. Corti (1994), Singular vectors and predictability of weather and climate, *Philos. Trans. R. Soc. London A*, *348*, 459–475.
Philander, S. G. H. (1983), El Niño southern oscillation phenomena, *Nature*, *302*(5906), 295–301.
Philander, S. G. H. (1990), *El Niño, La Niña and the Southern Oscillation*, 293 pp., Academic, San Diego, Calif.
Powell, M. J. D. (1982), VMCWD: A FORTRAN subroutine for constrained optimization, *DAMTP Rep. 1982/NA4*, Univ. of Cambridge, Cambridge, U. K.
Rasmusson, E. M., and T. H. Carpenter (1982), Variations in tropical sea surface temperature and surface wind fields associated with the Southern Oscillation/El Nino, *Mon. Weather Rev.*, *110*(5), 354–384.
Rodríguez-Fonseca, B., I. Polo, J. García-Serrano, T. Losada, Mohino, C. R. Mechoso, and F. Kucharski (2009), Are Atlantic Niños enhancing Pacific ENSO events in recent decades?, *Geophys. Res. Lett.*, *36*, L20705, doi:10.1029/2009GL040048.
Ropelewski, C. F., and M. S. Halpert (1987), Global and regional scale precipitation patterns associated with the El Niño Southern Oscillation, *Mon. Weather Rev.*, *115*(8), 1606–1626.
Rutt, I. C., M. Hagdorn, N. R. J. Hulton, and A. J. Payne (2009), The Glimmer community ice sheet model, *J. Geophys. Res.*, *114*, F02004, doi: 10.1029/2008GF001015.
Samelson, R. M., and E. Tziperman (2001), Instability of the chaotic ENSO: The growth-phase predictability barrier, *J. Atmos. Sci.*, *58*(23), 3613–3625.
Smith, T. M., W. R. Reynolds, T. C. Peterson, and J. Lawrimore (2008), Improvements to NOAA's historical merged land-ocean surface temperature analysis (1880–2006), *J. Clim.*, *21*, 2283–2296, doi:10.1175/2007JCLI2100.1.
Snyder, C. (1996), Summary of an informal workshop on adaptive observations and FASTEX, *Bull. Am. Meteorol. Soc.*, *77*, 953–961.
Thompson, C. J. (1998), Initial conditions for optimal growth in a coupled ocean-atmosphere model of ENSO, *J. Atmos. Sci.*, *55*, 537–557.
Tippett, M. K., A. G. Barnston, and S. H. Li (2012), Performance of recent multimodel ENSO forecasts, *J. Appl. Meteorol. Climatol.*, *51*, 637–654.
Trenberth, K. E., G. W. Branstator, D. Karoly, A. Kumar, N. C. Lau, and C. Ropelewski (1998), Progress during TOGA in understanding and modeling global teleconnections associated with tropical sea surface temperatures, *J. Geophys. Res.*, *103*, 14,291–14,324.
Vimont, D. J., M. A. Alexander, and M. Newman (2014), Optimal growth of Central and East Pacific ENSO events, *Geophys. Res. Lett.*, *41*, 4207–4034, doi:10.1002/2014GL059997.
Wen, C. H., A. Kumar, Y. Xue, and M. J. Mcphaden (2014), Changes in Tropical Pacific Thermocline Depth and Their Relationship to ENSO after 1999, *J. Clim.*, *27*(19), 7230–7249, doi:10.1175/JCLI-D-13-00518.1.
Wyrtki, K. (1975), El Niño-the dynamic response of the equatorial Pacific Ocean to atmospheric forcing, *J. Phys. Oceanogr.*, *5*, 572–584.
Wyrtki, K. (1985), Water displacements in the pacific and the genesis of El Niño cycles, *J. Geophys. Res.*, *90*, 7129–7132.
Xue, Y., M. A. Cane, S. E. Zebiak, and M. B. Blumenthal (1994), On the prediction of ENSO: A study with a low-order Markov model, *Tellus, Ser. A*, *46*(4), 512–528.
Yu, J. Y., and H. Paek (2015), Precursors of ENSO beyond the tropical Pacific, US CLIVAR Variations, *13*(1), 15–20. [Available at http://escholarship.org/uc/item/3rp5r9vq.]
Yu, Y. S., W. S. Duan, H. Xu, and M. Mu (2009), Dynamics of nonlinear error growth and season-dependent predictability of El Niño events in the Zebiak-Cane model, *Q. J. R. Meteorol. Soc.*, *135*, 2146–2160.
Zebiak, S. E., and M. A. Cane (1987), A Model El Niño Southern Oscillation, *Mon. Weather Rev.*, *115*(10), 2262–2278.
Zelle, H., G. Appeldoorn, G. Burgers, and G. J. van Oldenborgh (2004), The relationship between sea surface temperature and thermocline depth in the eastern equatorial Pacific, *J. Phys. Oceanogr.*, *34*(3), 643–655.
Zhu, J., A. Kumar, and B. Huang (2015), The relationship between thermocline depth and SST anomalies in the eastern equatorial Pacific: Seasonality and decadal variations, *Geophys. Res. Lett.*, *42*, 4507–4515, doi:10.1002/2015GL064220.